Title: A conserved membrane protein negatively regulates Mce1 complexes in mycobacteria

Authors: Yushu Chen[1], Yuchun Wang[1], Shu-Sin Chng[1,2]*

Affiliations:

[1] Department of Chemistry, National University of Singapore, Singapore 117543.

[2] Singapore Center for Environmental Life Sciences Engineering, National University of Singapore (SCELSE-NUS), Singapore 117456.

* To whom correspondence should be addressed. Email: chmchngs@nus.edu.sg

Abstract

Tuberculosis (TB) continues to pose a serious threat to global health. *Mycobacterium tuberculosis*, the causative agent of TB, is an intracellular pathogen that relies on various mechanisms to survive and persist within the host. Among their many virulence factors, mycobacteria encode Mce systems, putative transporters that are important for lipid uptake; the molecular basis for Mce function(s) is poorly understood. To gain insights into the composition and architecture of Mce systems, we characterized the putative Mce1 complex involved in fatty acid transport. We show that the Mce1 system in *Mycobacterium smegmatis* comprises a canonical ATP-binding cassette transporter, associated with functionally redundant heterohexameric assemblies of substrate-binding proteins. Furthermore, we establish that the conserved membrane protein Mce1N negatively regulates Mce1 function via a unique mechanism involving blocking transporter assembly. Our work offers molecular understanding of Mce complexes, sheds light on mycobacterial lipid metabolism and its regulation, and informs future anti-mycobacterial strategies.

Introduction

Tuberculosis (TB) has been one of the top killers among single infectious diseases in humans, alone claiming 1.4 million lives out of 10.6 million new cases in 2021 (1). Apart from the active cases, it is estimated that one quarter of the world population are carriers of latent TB, which may progress into active infections (2). TB is primarily caused by *Mycobacterium tuberculosis*, an organism known for its ability to adapt to the host environment and modulate the host immune system (3). Its success as a pathogen can be owed to diverse virulence factors encoded in the genome of *M. tuberculosis*. In particular, many of these virulence factors promote host adaptation by contributing to the acquisition and catabolism of important nutrients including metals, sugars and lipids (4).

Mycobacterial *mce* operons have been recognized as a group of virulence factors important for lipid uptake (5). These operons are widespread throughout the *Mycobacterium* genus, with different numbers present in different species (6). *Mycobacterium smegmatis,* an environmental microorganism, contains six *mce* operons*,* while *Mycobacterium leprae*, the causative agent of leprosy, has only one such operon (*mce1*) in its highly degenerate genome. *M. tuberculosis* contains four *mce* operons, individually important determinants of virulence and collectively critical for pathogenesis (7–10). For example, the *mce1* and *mce4* operons are implicated in fatty acid and cholesterol uptake, respectively (9, 11, 12). In general, an *mce* operon consists of eight genes, two *yrbE* (e.g., *yrbE1A/B*) and six *mce* genes (e.g., *mce1A–F),* with different numbers of accessory genes (6) that may be required for function (12, 13) (e.g., *mam1A–D* after the *mce1* operon). Furthermore, a gene encoding a transcriptional regulator (e.g., *mce1R*) can be found upstream of some *mce* operons (6, 14, 15) (Fig. 1A, Fig. S1). Our understanding of how these operons facilitate lipid uptake is limited.

It is believed that *mce* operons encode ATP-binding cassette (ABC) transporters that are analogous to the MlaFEDB complex in Gram-negative bacteria (6, 16), which is important for retrograde transport of phospholipids (17, 18). In MlaFEDB, MlaF, MlaE and MlaD represent the nucleotide-binding domains (NBDs), transmembrane domains (TMDs), and substrate-binding proteins (SBPs), respectively (19, 20). In Mce systems, YrbEA/Bs and MceA–Fs would form the corresponding TMDs and SBPs based on homology; here, MceG, a protein not encoded within *mce* operons, is thought to constitute the NBDs that energize all these putative transporters (21, 22). MlaD and MceA–F all contain a single mammalian cell entry (MCE)

domain. Interestingly, MlaD and other MCE-domain proteins, such as PqiB and YebT/LetB, have been shown to form homohexamers that provide a hydrophobic tunnel each, presumably for lipid substrate transport (19, 20, 23, 24). The fact that *mce* operons encode six Mce proteins MceA–F hints at the possible formation of heterohexameric MCE assemblies within each putative transporter. Despite similarities to MlaFEDB, however, there has been a lack of biochemical studies on mycobacterial Mce systems, and their exact compositions and overall architectures remain unknown.

Here, we biochemically characterized the putative Mce1 complex in *M. smegmatis.* We demonstrate that Mce1 is an ABC transporter comprising a core complex of YrbE1A/B-MceG, associated with a likely heterohexamer of Mce1A–F. We reveal that Msmeg_6540 is a functional homolog that can possibly replace Mce1A in the complex, and in fact, contributes more significantly to the fatty acid uptake function of Mce1. Furthermore, we identify Msmeg_0959, herein renamed to Mce1N, as a negative regulator of the Mce1 system; it prevents MceG from associating with the complex via competitive binding to YrbE1B, thereby modulating transport activity. Our work provides critical insights into the architecture, function and regulation of Mce systems in mycobacteria.

Results

Key proteins encoded in the *mce1* operon co-purify as a complex

To probe the composition of the putative Mce1 complex, we expressed His-tagged YrbE1A or YrbE1B in *M. smegmatis* using an integrative plasmid and conducted affinity purification following cell lysis and detergent extraction from total membranes. This was done in a strain that presumably up-regulates the *mce1* operon due to the lack of Mce1R, a known negative regulator (14). We found that His-tagged YrbE1B, but not YrbE1A, pulled down two distinct protein bands at ~45 and ~19 kDa (Fig. 1B). Tandem mass spectrometry (MS/MS) sequencing of the excised bands indicated that they were MceG (39.0 kDa) and a protein of unknown function, Msmeg_0959 (19.1 kDa), respectively. We did not observe additional bands corresponding to other expected members of the Mce1 complex, possibly due to low cellular levels, or instability of the complex *ex vivo*. To detect potential low abundance proteins specifically co-purified with His-tagged YrbE1B, we directly subjected entire gel lanes divided into two sections to MS/MS protein identification. Remarkably, this facilitated the detection of all other putative Mce1 components, including

YrbE1A and Mce1A–F, similar to a recent report identifying YrbE4A/B, Mce4A–F and MceG as components of the Mce4 complex (13). Interestingly, a seventh MCE-domain protein Msmeg_6540 (6) was also co-purified with His_6-YrbE1B, while none of the putative Mce-associated membrane proteins (Mam1A–D) was identified. Our data suggest that the Mce1 complex likely comprises the core ABC transporter YrbE1A/B-MceG associated with a presumed heterohexamer of MCE-domain proteins.

Msmeg_6540 and Mce1A are two redundant components of the Mce1 system

Msmeg_6540 shares 80% primary sequence identity with Mce1A, compared to less than 20% with other MCE-domain proteins in the Mce1 complex and ~25% with MceA proteins in other putative *M. smegmatis* Mce complexes (Table S1). Another Mce1A paralog Msmeg_5818 (6), which is only 60% identical, was not co-purified with His-tagged YrbE1B (Fig. 1B). This suggests that Msmeg_6540 could be a functional homolog of Mce1A. To study the role of Msmeg_6540, we tested the effects of deleting *msmeg_6540* on fatty acid uptake, a key function of the Mce1 complex (11, 12). Deletion of *yrbE1A/B*, or *mceG* resulted in reduced [^{14}C]-palmitic acid uptake (Fig. 2A, Fig. S2), and retarded cell growth specifically when palmitate was the sole carbon source (Fig. 2B). Interestingly, we found that [^{14}C]-palmitic acid uptake was less efficient in cells lacking either *mce1A* or *msmeg_6540*, and only further reduced to baseline in the Δ*mce1A*Δ*6540* double mutant, i.e. at levels of Δ*yrbE1A/B* cells (Fig. 2A). In addition, while both single deletion mutants exhibited slower growth when using palmitate as the sole carbon source, the Δ*mce1A*Δ*6540* strain grew at an even lower rate, again similar to Δ*yrbE1A/B* or Δ*mceG* strains (Fig. 2B). Our results therefore reveal that Mce1A and Msmeg_6540 are functionally redundant, and may somewhat replace each other in Mce1 complexes. We note that removing Msmeg_6540 has a much stronger impact on fatty acid uptake than removing Mce1A (Fig. 2A). In fact, expressing *msmeg_6540*, but not *mce1A*, could almost fully complement the Δ*mce1A*Δ*6540* strain (Fig. 2C). Importantly, it appears that removing other MCE-domain proteins in the complex, e.g., Mce1F, resulted in complete loss of Mce1 function (Fig. 2D). We conclude that Mce1A and Msmeg_6540 exist in distinct heterohexamers together with Mce1B–F, with the latter complex playing a more important role in fatty acid uptake in *M. smegmatis*.

YrbE1A/B-MceG constitute the core ABC transporter

Despite extensive efforts, we were not successful in over-expressing the *mce1* operon along with *mceG* in *E. coli* and purifying the full Mce1 complex. Instead, we were able to isolate the core ABC transporter when we co-expressed YrbE1A, His-tagged YrbE1B and MceG. This complex eluted as a single peak on size exclusion chromatography (Fig. 3A); we showed that the purified complex exhibits ATP hydrolytic activity (Fig. 3B), implying proper assembly of YrbE1A/B-MceG. Interestingly, we found that His-tagged YrbE1B alone could pull down MceG when co-expressed in *E. coli*. In contrast, His-tagged YrbE1A could only co-purify with MceG in the presence of YrbE1B, indicating that the TMD-NBD interactions are mainly mediated through YrbE1B (Fig. 3C). Consistent with this idea, an AlphaFold2 structural model of the YrbE1A/B-MceG complex (25–27), which resembles the homologous MlaFE structure from Gram-negative bacteria (RMSD=2.934 Å) (28), presented a smaller buried area between MceG and YrbE1A (699 $Å^2$) compared to YrbE1B (837 $Å^2$) (Fig. S3, Table S2). We conclude that the TMDs and NBD proteins of the Mce1 system interact asymmetrically to form a stable functional ABC transporter.

Msmeg_0959 is a negative regulator of Mce1

In addition to MceG, Msmeg_0959 was another protein abundantly co-purified with His-tagged YrbE1B expressed in *M. smegmatis*. Msmeg_0959 is a putative conserved membrane protein with unknown function; it contains two predicted transmembrane helices (TM1: W39–G59; TM2: L65–T90) and a C-terminal cytoplasmic domain (S91–P178) (Fig. S4A). We initially hypothesized that it might function to stabilize the Mce1 complex, analogous to the role of the cytoplasmic protein MlaB in the Gram-negative MlaFEDB complex (19). To test this idea, we attempted to isolate a stable complex containing YrbE1A/B, MceG and Msmeg_0959. To our surprise, when these four proteins were co-expressed and purified from *E. coli*, only Msmeg_0959 was co-purified with His-tagged YrbE1B (Fig. 4A). We detected much less YrbE1A and essentially no MceG co-purified, suggesting that Msmeg_0959 may destabilize the Mce1 complex instead. In support of this notion, when Msmeg_0959 was overexpressed in *M. smegmatis*, much less MceG was co-purified with His-tagged YrbE1B (Fig. 4C). We conclude that Msmeg_0959 may disrupt YrbE1A/B-MceG interactions.

Since TMD-NBD interaction within the Mce1 complex is largely mediated through YrbE1B, we presumed that Msmeg_0959 directly interacts with YrbE1B. Indeed, His-tagged YrbE1B alone, but not

YrbE1A, pulled down Msmeg_0959 when co-expressed in *E. coli*, consistent with affinity purification results in *M. smegmatis* (Fig. 1, Fig. S5A and B). We generated an AlphaFold2 structural model comprising YrbE1B and Msmeg_0959 (25–27), predicting possible interactions between the transmembrane domain of Msmeg_0959 and that of YrbE1B opposite its dimerization surface with YrbE1A (Fig. 4D). To test the validity of this model, we introduced cysteine pairs across potential contact sites in the transmembrane regions of the two proteins, and looked for disulfide bond formation when these variants are expressed in *E. coli*. Five pairs of cysteines at the periplasmic side of the putative interface enabled crosslinking between YrbE1B and Msmeg_0959 (Fig. 4E, Fig. S6), lending confidence to the predicted interaction mode. The AlphaFold2 model revealed that an unstructured loop in the cytoplasmic domain of Msmeg_0959 may contact a short helix of YrbE1B sitting at the membrane-water boundary. This helix may be a determinant of the interaction between YrbE1B and Msmeg_0959 since the amino acid sequence of this region is very different from that in YrbE1A (Fig. S5C). Mutating part of this helix (RLVAEIGMGT) to a flexible loop (GGSSG) did not affect the stability of the YrbE1A/B-MceG complex; however, this mutation prevented co-purification of Msmeg_0959 with His-tagged YrbE1B from *E. coli*, at the same time alleviating the destabilizing effect of Msmeg_0959 on YrbE1A/B-MceG interactions (Fig. 4A). Notably, overlay of the models of YrbE1B-Msmeg_0959 and YrbE1A/B-MceG highlighted substantial steric clashes between MceG and the cytoplasmic domain of Msmeg_0959 (Fig. 4D), indicating that their respective interactions with YrbE1B are likely competitive and mutually exclusive. We also generated an Msmeg_0959 variant (Msmeg_0959$_{AGG3P}$) where the cytoplasmic loop that appears to interact with YrbE1B is modified (^{131}ALGELTG to PLPELTP) to impact overall conformation. Intriguingly, this variant still interacts with YrbE1B but is no longer able to compete out MceG when co-expressed in either *E. coli* (Fig. 4B) or *M. smegmatis* (Fig. 4C). Taken together, our results establish that Msmeg_0959 specifically binds YrbE1B and prevents association of the NBD (MceG) to this ABC transporter.

Our biochemical experiments suggest that Msmeg_0959 may be a negative regulator of the Mce1 complex. Consistent with this idea, Msmeg_0959 overexpression inhibited [^{14}C]-palmitic acid uptake in WT cells, but not residual uptake observed in Δ*yrbE1A/B* cells (Fig. 4F). In contrast, overexpression of Msmeg_0959$_{AGG3P}$ did not inhibit [^{14}C]-palmitic acid uptake at all (Fig. 4F), in line with its inability to displace MceG (Fig. 4C). Furthermore, we found that overexpression of Rv0513, the *M. tuberculosis*

homolog of Msmeg_0959, reduced the amount of MceG associated with YrbE1B (Fig. 4C) in *M. smegmatis*, and slowed down [^{14}C]-palmitic acid uptake (Fig. 4F). We therefore conclude that Msmeg_0959/Rv0513, herein renamed to Mce1N (Mce1 negative regulator), inhibits the fatty acid uptake function of the Mce1 transporter(s) via a conserved mechanism that involves prevention of YrbE1B-MceG interaction.

Discussion

In this study, we set out to characterize the Mce1 complex in *M. smegmatis*. We have shown that the complex likely comprises the core inner membrane ABC transporter YrbE1A/B-MceG, associated with a putative heterohexamer composed of Mce1A–F. Interestingly, we have found that Msmeg_6540, a homolog of Mce1A, can also be co-purified as part of the Mce1 complex, and have demonstrated that it is functionally redundant with Mce1A in fatty acid uptake. Furthermore, we have discovered a negative regulator of the Mce1 complex, Mce1N, which physically hinders the dominant TMD-NBD interaction (i.e., YrbE1B-MceG) in the ABC transporter. Our work provides novel insights into the architecture and regulation of mycobacterial Mce complexes.

Based on analogy to other MCE-domain proteins, such as MlaD, PqiB (20) and YebT/LetB (23, 24) involved in lipid transport in Gram-negative bacteria (Fig. S7A), Mce1A–F likely form a hexamer. Each of these Mce proteins contains a single MCE domain (like MlaD) and an extended helical domain (like PqiB), followed by the presence of an additional C-terminal domain of varied sizes. According to AlphaFold2 prediction (25, 26, 29), Mce1A–F can indeed form a heterohexamer (Fig. S7B). In contrast, a homohexameric model of Mce1A alone could not be generated. In the AlphaFold2 model, the heterohexamer adopts an architecture that comprises a hexameric MCE ring connected to a tube formed by a bundle of the helical domains; the C-terminal domains of the six Mce proteins organize to form a possible substrate entry point at the very tip (Fig. S7B). A continuous hydrophobic tunnel runs through the entire assembly that likely extends across the periplasm to contact the mycobacterial outer membrane (Fig. 5, Fig. S7B and C), consistent with its function in fatty acid uptake. This predicted model resembles the recently solved cryo-electron microscopy (EM) structure of the Mce1 complex remarkably well (30). Interestingly, *M. smegmatis* possesses Msmeg_6540 as a functional homolog of Mce1A, hinting towards the presence of two variants of Mce1 complexes (6), containing Mce1B–F and either Mce1A or Msmeg_6540 (Fig. 5). In

support of this idea, deleting *mce1F*, but not *mce1A* or *msmeg_6540* alone, completely abolishes Mce1 function in fatty acid uptake (Fig. 2A and C). Differences between the primary sequences of Mce1A and Msmeg_6540 lie mainly in the extreme C-terminal domain, with differing residues primarily mapped to the substrate entry point in the AlphaFold2 models (Fig. S7D). We propose that Mce1 complexes containing either Mce1A or Msmeg_6540 may have distinct substrate specificities, perhaps advantageous for an environmental microorganism like *M. smegmatis*.

Despite the fact that there are known ABC transporters with heterodimeric TMDs, it has not been appreciated that such asymmetry can give rise to major differences in affinity between each TMD and NBD pair—in the case of the Mce1 transporter, the NBD dimer may be predominantly recruited by YrbE1B (Fig. 3C). This might be applicable to other ABC transporters with heterodimeric TMDs since TMD-NBD interfaces of different areas were also observed within some of them (Table S2). That TMD-NBD association in the Mce1 transporter relies on the YrbE1B-MceG interaction offers a compelling reason why the negative regulator Mce1N also selectively binds YrbE1B (Fig. 1B, Figure S5A and B). Based on our modeling and biochemical data (Fig. 4A and D), the cytoplasmic domain of Mce1N likely interacts with YrbE1B extensively at a short helix between the latter's N-terminal amphipathic interface helix and TM1. This short helix is nominally a part of TM1 but is presented at an angle due to a kink introduced by a flexible loop within TM1. Remarkably, this structural feature may be exclusively conserved across YrbEBs, but not YrbEAs (Fig. S8). This raises an interesting possibility that beyond the most conserved Mce1 complex, Mce1N may also regulate additional Mce systems by binding to the corresponding YrbEB, perhaps providing a way to redistribute MceG among all Mce systems.

The discovery of a negative regulator that competes with the NBD for binding to the TMDs may be unique to Mce complexes, as known regulatory mechanisms for ABC transporters typically involve modulation of ATPase activity instead of removing the NBD from the complex (19, 31–35). How and when the Mce1 complex is modulated would directly depend on the levels of Mce1N (Fig. 5), which is highly conserved across the *Mycobacterium* genus (present in both fast- and slow-growing, pathogenic and non-pathogenic species). We note that *mce1N* may be in an operon together with four upstream essential genes involved in porphyrin biosynthesis (*hemACDB*). Porphyrin biosynthesis has been reported to increase, suggesting possible up-regulation of Mce1N (Msmeg_0959), when *M. smegmatis* cells enter dormancy (36).

In this situation, negative regulation by Mce1N might be a strategy that cells use to inhibit some Mce complexes to conserve ATP. Alternatively, Mce1N levels may correlate with the need for lipid uptake. Outside the host, where fatty acid substrates may be scarce, it might be preferable for mycobacterial cells to keep the Mce1 system in a routinely OFF state and avoid futile ATP hydrolysis. During infection, however, cells may require a fully active Mce1 complex to utilize host fatty acids. We do not yet know of any environment-dependent regulation of Mce1N. However, it is noteworthy that in *M. leprae,* which possesses Mce1 as the only Mce system (6), Mce1N (Ml2418c) lacks the C-terminal cytoplasmic domain (Fig. S4B) and is likely non-functional. Combined with the fact that *mce1R,* the gene encoding the transcriptional repressor of the *mce1* operon (Fig. S1), is absent in *M. leprae*, the pathogen may have lost its ability to down-regulate the Mce1 system, which can facilitate constitutive fatty acid uptake during its obligate parasitic life cycle.

We have uncovered a new regulatory mechanism for Mce1 (Fig. 5), and potentially other Mce systems, which may have implications for how mycobacterial cells coordinate lipid uptake processes. Despite the presence of a transcriptional regulator for some *mce* operons (Fig. S7), all Mce transporters apparently share the same ATPase MceG (22). This indicates that mycobacterial cells have the ability to modulate the levels of each complex, yet adjust their activities simultaneously. In the same vein, we speculate that Mce1N could also be a shared negative regulator to counter MceG binding/activation, and primarily functions to deactivate all Mce complexes simultaneously. Whether Mce1N has preferences for specific Mce systems remains to be examined. Nevertheless, it likely contributes significantly to the overall regulation towards maintaining a balanced metabolic flux of different lipid substrates required for mycobacterial survival (12, 37), which may involve other yet-to-be-identified uptake transporters beyond Mce systems (38).

Materials and Methods

Construction of *M. smegmatis* knock-out strains

M. smegmatis strains used in this study are listed in Table S1. The knockout strains were constructed by two-step homologous recombination as reported previously (39). Briefly, a suicide plasmid pYUB854 with no replication origin and a *hygR* cassette was used as the backbone for insertion of two flanking regions of the target gene side by side, and a *lacZ-sacB* cassette for blue-white screening and negative selection on

251 sucrose. The plasmid was electroporated at 2250 V using Eporator (Eppendorf) into *M. smegmatis* mc^{2}155
252 electrocompetent cells, which were subsequently plated on LB plates containing 50 μg/mL hygromycin and
253 20 μg/mL 5-bromo-4-chloro-3-indolyl-β-D-galactopyranoside (X-gal). The plate was incubated at 37 ºC
254 for 5–7 days to allow the growth of first cross-over cells (those forming blue colonies on the plate). Cells
255 harboring the first cross-over at the targeted site were grown in 7H9 medium containing 0.5% glycerol and
256 0.05% tyloxapol and spread onto LB plates containing 20 μg/mL X-gal and 5% sucrose. The plate was
257 again incubated at 37 ºC for 4 days to allow the growth of second cross-overs (those forming whitish-yellow
258 colonies on the plate). Correct gene deletion mutants were screened by PCR and Sanger sequencing (Bio
259 Basic Asia Pacific, Singapore) among the second cross-overs.
260
261 **Pull-down assay in *M. smegmatis***
262 Plasmids used in this study for protein expression in *M. smegmatis* are listed in Table S2. pJEB402 or
263 pMV306hsp vectors carrying genes of interest were transformed into *M. smegmatis* cells by electroporation.
264 The cells were grown in 750 mL tryptic soy broth supplemented with 0.05% Tween 80 to stationary phase
265 (OD_{600} ~5) and harvested by centrifugation at 4,800 xg for 10 min. Harvested cells were resuspended in
266 cold 20 mL TBS (Tris-buffered saline, 20 mM Tris-HCl pH 8.0, 150 mM NaCl) containing 100 μg/mL
267 lysozyme, 100 μM phenylmethylsulfonyl fluoride, and 50 μg/mL DNase I, and lysed by two passages
268 through a French Press (GlenMills) at 18,000 psi. The resulting suspension was centrifuged at 4,800 xg for
269 4 min to remove unbroken cells. The supernatant containing the cell lysate was subjected to centrifugation
270 at 95,000 xg for 45 min. The pelleted membrane was resuspended in 5 mL extraction buffer (TBS pH 8.0
271 containing 5 mM $MgCl_2$, 10% glycerol, 5 mM imidazole, and 1% n-dodecyl-β-D-maltoside (DDM)) and
272 extracted on ice with gentle shaking for 2 h. The suspension was subjected to a second round of
273 centrifugation at 89,000 xg for 45 min. The supernatant was loaded onto 100 μL TALON metal affinity
274 resin (Takara Bio) pre-equilibrated with TBS pH 8.0 containing 10 mM imidazole. The mixture was allowed
275 to drain by gravity and the filtrate was loaded back to the column and drained again. The resin was washed
276 with 500 μL washing buffer (20 mM Tris-HCl pH 8.0, 300 mM NaCl, 5 mM $MgCl_2$, 10% glycerol, 8 mM
277 imidazole, and 0.05% DDM) for ten times and subsequently eluted with 100 μL elution buffer (TBS pH 8.0
278 containing 5 mM $MgCl_2$, 10% glycerol, 200 mM imidazole, and 0.05% DDM) for four times. The eluate

was concentrated using an Amicon Ultra 10 kDa centrifugal filter (MilliporeSigma) and kept for further SDS-PAGE analysis. Protein gel sections and bands to be identified were sent to Taplin Biological Mass Spectrometry Facility, Harvard Medical School (Boston, MA) for capillary LC-MS/MS analysis.

Protein purification from *E. coli*

Plasmids used in this study for protein expression in *E. coli* are listed in Table S3. *E. coli* BL21(λDE3) cells were used as the host strain. Cells were grown to OD_{600} = 0.6 in 1.5 L LB broth, before 1 mM IPTG was added to induce expression of the proteins for 2 h. The cells were harvest by centrifugation at 4,800 xg for 10 min. Harvested cells were resuspended in cold 20 mL TBS (Tris-buffered saline, 20 mM Tris-HCl pH 8.0, 150 mM NaCl) containing 100 µg/mL lysozyme, 100 µM phenylmethylsulfonyl fluoride, and 50 µg/mL DNase I, and lysed by two passages through a French Press at 18,000 psi. The resulting suspension was centrifuged at 4,800 xg for 4 min to remove unbroken cells. The supernatant containing the cell lysate was subjected to centrifugation at 95,000 xg for 45 min. The pelleted membrane was resuspended in the 5 mL extraction buffer (TBS pH 8.0 containing 5 mM $MgCl_2$, 10% glycerol, 5 mM imidazole, and 1% DDM) and extracted on ice with gentle shaking for 2 h. The suspension was subjected to a second round of centrifugation at 89,000 xg for 45 min. The supernatant was loaded onto TALON metal affinity resin (Takara Bio) pre-equilibrated with TBS pH 8.0 containing 10 mM imidazole. The mixture was allowed to drain by gravity and the filtrate was loaded back to the column and drained again. The resin was washed 10 times with the washing buffer (20 mM Tris-HCl pH 8.0, 300 mM NaCl, 5 mM $MgCl_2$, 10% glycerol, 8 mM imidazole, and 0.05% DDM) and subsequently eluted with the elution buffer (TBS pH 8.0 containing 5 mM $MgCl_2$, 10% glycerol, 200 mM imidazole, and 0.05% DDM). The eluate was concentrated using an Amicon Ultra 10 kDa centrifugal filter (MilliporeSigma) and subjected to SDS-PAGE analysis. YrbE1A/B-MceG and YrbE1A/B-$MceG_{K43A}$ were further purified and analyzed by SEC (AKTA, GE Healthcare) at 4 ºC on a pre-packed Superdex Increase 200 10/300 GL column (Cytiva). TBS pH 8.0 containing 5 mM $MgCl_2$, 10% glycerol, and 0.05% DDM was used as the eluent. Fractions corresponding to the peaks of our interest were concentrated and subjected to SDS-PAGE analysis.

SDS-PAGE and Western Blotting

307 Protein samples were mixed with Laemmli buffer and analyzed by Tris-glycine SDS-PAGE. The gel
308 was visualized by InstantBlue Coomassie Blue Stain (Abcam) or subjected to Western blotting. For the
309 latter, the proteins on the gel were transferred to a polyvinylidene fluoride membrane using a Transblot SD
310 semi-dry transfer system (BioRad) at 25V for 30 min. The membrane was blocked in 1x casein blocking
311 buffer for at least 1 h. For detection of His-tagged proteins, a conjugate of mouse monoclonal penta-His
312 antibody and horseradish peroxidase (Qiagen) was used. For detection of FLAG-tagged proteins, a
313 conjugate of mouse monoclonal FLAG-antibody and horseradish peroxidase (MilliporeSigma) was used.
314 To visualize the blots, Luminata Forte Western HRP Substrate (MilliporeSigma) was applied to the
315 membrane.
316
317 **Disulfide bond analysis**
318 His_6-YrbE1B and Msmeg_0959-FLAG were overexpressed in *E. coli* BL21(λDE3) cells harboring
319 pET28b*his*$_6$*-yrbE1B* and pCDFduet*msmeg_0959-FLAG*, with site-specific cysteine substitutions. The cells
320 were grown to OD_{600} = 0.6 in LB broth, before 1 mM IPTG was added to induce expression of the proteins
321 for 2 h. The cells were harvest by centrifugation at 4,000 xg for 3 min. The pellets were resuspended in 2x
322 Laemmeli buffer with (for reducing conditions) or without (for non-reducing conditions) 10% β-
323 mecaptoethanol. The samples were centrifuged at 21,000 xg for 10 min before being subjected to SDS-
324 PAGE and immunoblot analyses.
325
326 **Determination of cell growth in different media**
327 *M. smegmatis* cells were grown in 7H9 medium (Middlebrook) containing 0.5% glycerol and 0.05%
328 tyloxapol to an OD_{600} around 2. The cells were subcultured into the same 7H9 medium or into Sauton's
329 medium (0.5 g/L K_2HPO_4, 0.25 g/L $MgSO_4$, 2 g/L citric acid, 0.4 g/L L-asparagine, 0.05 g/L ferric
330 ammonium citrate, 5 g/L fatty acid-free bovine serum albumin, 0.05% tyloxapol, pH 7.0) containing
331 palmitic acid as the sole carbon source. The starting OD_{600} for the subculture was 0.001 for the 7H9 medium
332 and 0.0001 for the Sauton's medium. To prepare the Sauton's medium, palmitic acid was dissolved in 0.1
333 M NaOH, heated to 80 ºC and added into the medium with constant stirring to a final concentration of 300
334 μM. The cultures were incubated at 37 ºC with 200 rpm shaking. Growth of the cells were monitored at

specified time points using a UV-Vis spectrophotometer at 600 nm.

Palmitic acid uptake assay

The palmitic acid uptake assay was adapted from (12). *M. smegmatis* cells were grown in 7H9-glycerol-tyloxapol medium until the stationary phase and sub-cultured into Sauton's medium with palmitate as the carbon source. Stationary-phase cells (OD ~0.4) were pelleted by centrifugation at 3,000 xg for 4 min and resuspended in 1xPBS supplemented with 0.05% Triton X-100 and 0.1% fatty acid-free bovine serum albumin (BSA) yielding a final OD_{600} of 0.8. [^{14}C]-palmitic acid (Perkin Elmer) was added to a final activity concentration of 0.2 µCi/mL. The cells were incubated at 37 ºC with 200 rpm shaking. Cells were harvested at different time points (5, 15, 30, 45 min) by centrifugation at 5,000 xg for 1 min from 300 µL suspension and washed once with ice-cold PBS containing Triton X-100 and BSA. The cells were finally resuspended in the same buffer and aliquoted into three plastic scintillation vials for counting using a MicroBeta2 microplate counter (Perkin Elmer).

Enzyme-coupled ATPase assay

ATP hydrolytic activity was measured using an NADH-coupled assay (40) adapted for plate readers (41), as previously described (19). Each 50 µL reaction is made up of 20 mM Tris-HCl pH 8.0, 150 mM NaCl, 5 mM MgCl2 ,10% glycerol, 0.05% DDM, 200 mM NADH (MilliporeSigma), 20 U/mL lactic dehydrogenase (MilliporeSigma), 100 U/mL pyruvate kinase (MilliporeSigma), 0.5 mM phosphoenolpyruvate (MilliporeSigma) and various ATP (MilliporeSigma) concentrations. Protein complexes were added to a final concentration of 0.1 µM. Fluorescence emission at 340 nm from the reaction mixture was monitored at 37°C with 15 s intervals using a Biotek Synergy H1 microplate reader equipped with Biotek Gen5 software (Agilent). A linear fit was performed for the measured fluorescence within 10 min reaction time to obtain the rate of decrease in NADH fluorescence, which was converted to ATP hydrolysis rates using a standard curve obtained with known ADP concentrations. The assay for each sample was performed in technical triplicates and the data were fit to the built-in Hill equation in OriginPro 2018b.

Bioinformatic and structural analyses

Topological prediction for Msmeg_0959 was done using the CCTOP server (http://cctop.ttk.hu/). Sequence alignment of proteins was done using pairwise (EMBOSS needle) or multiple sequence alignment (Clustal Omega) tools provided by EMBL-EBI (https://www.ebi.ac.uk/services). Structural prediction for YrbE1A/B-MceG, YrbEA/Bs-Msmeg_0959 was done using ColabFold (27) on the Colaboratory server (Google). Prediction for Mce hexamers was done using the AlphaFold multimer tool on the COSMIC[2] platform (28-29). For both predictions, no template information was used and Amber was used for relaxing the predicted models. Other settings were kept as default. Visualization of structures and overlay of structural models were performed using PyMOL 2.3.0. Interface analysis was performed using ChimeraX 1.4.

References

1. World Health Organization, "Global Tuberculosis Report 2022", (2022; https://www.who.int/publications/i/item/9789240061729).
2. R. M. Houben, P. J. Dodd, The global burden of latent tuberculosis infection: a re-estimation using mathematical modelling. *PLoS Med.* **13**, e1002152 (2016).
3. Q. Chai, Y. Zhang, C. H. Liu, *Mycobacterium tuberculosis*: an adaptable pathogen associated with multiple human diseases. *Front. Cell. Infect. Microbiol.* **8**, 158 (2018).
4. M. A. Forrellad, L. I. Klepp, A. Gioffré, J. S. y García, H. R. Morbidoni, M. de la P. Santangelo, A. A. Cataldi, F. Bigi, Virulence factors of the *Mycobacterium tuberculosis* complex. *Virulence* **4**, 3-66 (2013).
5. L. I. Klepp, J. S. y García, F. Bigi, Mycobacterial MCE proteins as transporters that control lipid homeostasis of the cell wall. *Tuberculosis (Edinb)* **132**, 102162 (2022).
6. N. Casali, L. W. Riley, A phylogenomic analysis of the *Actinomycetales mce* operons. *BMC Genomics* **8**, 60 (2007).
7. N. Shimono, N. Shimono, L. Morici, N. Casali, S. Cantrell, B. Sidders, S. Ehrt, L. W. Riley, Hypervirulent mutant of *Mycobacterium tuberculosis* resulting from disruption of the *mce1* operon. *Proc. Natl. Acad. Sci. U. S. A.* **100**, 15918-15923 (2003).
8. A. Gioffre, E. Infante, D. Aguilar, M. P. Santangelo, L. Klepp, A. Amadio, V. Meikle, I. Etchechoury,

M. I. Romano, A. Cataldi, R. P. Hernández, F. Bigi, Mutation in *mce* operons attenuates *Mycobacterium tuberculosis* virulence. *Microbes Infect.* **7**, 325-334 (2005).

9. A. K. Pandey, C. M. Sassetti, Mycobacterial persistence requires the utilization of host cholesterol. *Proc. Natl. Acad. Sci. U. S. A.* **105**, 4376-4380 (2008).
10. R. H. Senaratne, B. Sidders, P. Sequeira, G. Saunders, K. Dunphy, O. Marjanovic, J. R. Reader, P. Lima, S. Chan, S. Kendall, J. McFadden, L. W. Riley, *Mycobacterium tuberculosis* strains disrupted in *mce3* and *mce4* operons are attenuated in mice. *J. Med. Microbiol.* **57**, 164-170 (2008).
11. M. A. Forrellad, M. McNeil, M. de la P. Santangelo, F. C. Blanco, E. García, L. I. Klepp, J. Huff, M. Niederweis, M. Jackson, F. Bigi, Role of the Mce1 transporter in the lipid homeostasis of *Mycobacterium tuberculosis*. *Tuberculosis (Edinb)* **94**, 170-177 (2014).
12. E. V. Nazarova, C. R. Montague, T. La, K. M. Wilburn, N. Sukumar, W. Lee, S. Caldwell, D. G. Russell, B. C. VanderVen, Rv3723/LucA coordinates fatty acid and cholesterol uptake in *Mycobacterium tuberculosis*. *eLife* **6** (2017).
13. L. Rank, L. E. Herring, M. Braunstein, Evidence for the mycobacterial mce4 transporter being a multiprotein complex. *J. Bacteriol.* **203**, e00685-00620 (2021).
14. N. Casali, A. M. White, L. W. Riley, Regulation of the *Mycobacterium tuberculosis mce1* operon. *J. Bacteriol.* **188**, 441-449 (2006).
15. M. P. Santangelo, F. C. Blanco, M. V. Bianco, L. I. Klepp, O. Zabal, A. A. Cataldi, F. Bigi, Study of the role of Mce3R on the transcription of *mce* genes of *Mycobacterium tuberculosis*. *BMC Microbiol.* **8**, 38 (2008).
16. J. C. Malinverni, T. J. Silhavy, An ABC transport system that maintains lipid asymmetry in the Gram-negative outer membrane. *Proc. Natl. Acad. Sci. U. S. A.* **106**, 8009-8014 (2009).
17. X. Tang, S. Chang, K. Zhang, Q. Luo, Z. Zhang, T. Wang, W. Qiao, C. Wang, C. Shen, Z. Zhang Z, X. Zhu, X. Wei, C. Dong, X. Zhang, H. Dong, Structural basis for bacterial lipoprotein relocation by the transporter LolCDE. *Nat. Struct. Mol. Biol.* **28**, 347-355 (2021).
18. W.-Y. Low, S. Thong, S.-S. Chng, ATP disrupts lipid-binding equilibrium to drive retrograde transport critical for bacterial outer membrane asymmetry. *Proc. Natl. Acad. Sci. U. S. A.* **118** (2021).
19. S. Thong, B. Ercan, F. Torta, Z. Y. Fong, H. Y. Wong, M. R. Wenk, S. -S. Chng, Defining key roles for

auxiliary proteins in an ABC transporter that maintains bacterial outer membrane lipid asymmetry. *eLife* **5** (2016).

20. D. C. Ekiert, G. Bhabha, G. L. Isom, G. Greenan, S. Ovchinnikov, I. R. Henderson, J. S. Cox, R. D. Vale, Architectures of Lipid Transport Systems for the Bacterial Outer Membrane. *Cell* **169**, 273-285 e217 (2017).
21. S. M. Joshi, A. K. Pandey, N. Capite, S. M. Fortune, E. J. Rubin, C. M Sassetti, Characterization of mycobacterial virulence genes through genetic interaction mapping. *Proc Natl Acad Sci U S A* **103**, 11760-11765 (2006).
22. J. Garcia-Fernández, K. Papavinasasundaram, B. Galán, C. M. Sassetti, J. L. García, Unravelling the pleiotropic role of the MceG ATPase in *Mycobacterium smegmatis*. *Environ. Microbiol.* **19**, 2564-2576 (2017).
23. C. Liu, J. Ma, J. Wang, H. Wang, L. Zhang, Cryo-EM structure of a bacterial lipid transporter YebT. *J. Mol. Biol.* **432**, 1008-1019 (2020).
24. G. L. Isom, N. Coudray, M. R. MacRae, C. T. McManus, D. C. Ekiert, G. Bhabha, LetB structure reveals a tunnel for lipid transport across the bacterial envelope. *Cell* **181**, 653-664 (2020).
25. R. Evans *et al*., Protein complex prediction with AlphaFold-Multimer. Preprint at https://www.biorxiv.org/content/10.1101/2021.10.04.463034v2 (2022).
26. J. Jumper, R. Evans, A. Pritzel, T. Green, M. Figurnov, O. Ronneberger, K. Tunyasuvunakool, R. Bates, A. Žídek, A. Potapenko, A. Bridgland, C. Meyer, S. A. A. Kohl, A. J. Ballard, A. Cowie, B. Romera-Paredes, S. Nikolov, R. Jain, J. Adler, T. Back, S. Petersen, D. Reiman, E. Clancy E, M. Zielinski, M. Steinegger, M. Pacholska, T. Berghammer, S. Bodenstein, D. Silver, O. Vinyals, A. W. Senior, K. Kavukcuoglu, P. Kohli, D. Hassabis, Highly accurate protein structure prediction with AlphaFold. *Nature* **596**, 583-589 (2021).
27. M. Mirdita, K. Schütze, Y. Moriwaki, L. Heo, S. Ovchinnikov, M. Steinegger, ColabFold: making protein folding accessible to all. *Nat. Methods* **19**, 679-682 (2022).
28. C. Zhou, H. Shi, M. Zhang, L. Zhou, L. Xiao, S. Feng, W. Im, M. Zhou, X. Zhang, Y. Huang. Structural insight into phospholipid transport by the MlaFEBD complex from *P. aeruginosa*. *J. Mol. Biol.* **433**, 166986 (2021).

29. M. A. Cianfrocco, M. Wong, C. Youn, R. Wagner, A. E. Leschziner, "COSMIC²: A science gateway for cryo-electron microscopy structure determination" in *Proceedings of the Practice and Experience in Advanced Research Computing 2017 on Sustainability, Success and Impact* (Association for Computing Machinery, New York, NY, 2017), pp. 1-5.
30. J. Chen *et al*., Structure of an endogenous mycobacterial MCE lipid transporter. Preprint at https://www.biorxiv.org/content/10.1101/2022.12.08.519548v2 (2022).
31. R. R. Crawford, P. K. Potukuchi, E. G. Schuetz, J. D. Schuetz, Beyond competitive inhibition: regulation of ABC transporters by kinases and protein-protein interactions as potential mechanisms of drug-drug interactions. *Drug Metab. Dispos.* **46**, 567-580 (2018).
32. N. S. Kadaba, J. T. Kaiser, E. Johnson, A. Lee, D. C. Rees, The high-affinity *E. coli* methionine ABC transporter: structure and allosteric regulation. *Science* **321**, 250-253 (2008).
33. S. Gerber, M. Comellas-Bigler, B. A. Goetz, K. P. Locher, Structural basis of trans-inhibition in a molybdate/tungstate ABC transporter. *Science* **321**, 246-250.
34. S. Chen, M. L. Oldham, A. L. Davidson, J. Chen, Carbon catabolite repression of the maltose transporter revealed by X-ray crystallography. *Nature* **499**, 364-368 (2013).
35. S. B. Ko, W. Zeng, M. R. Dorwart, X. Luo, K. H. Kim, L. Millen, H. Goto, S. Naruse, A. Soyombo, P. J. Thomas, S. Muallem, Gating of CFTR by the STAS domain of SLC26 transporters. *Nat. Cell. Biol.* **6**, 343-350 (2004).
36. V. D. Nikitushkin, M. O. Shleeva, A. I. Zinin, K. A. Trutneva, D. N. Ostrovsky, A. S. Kaprelyants, The main pigment of the dormant *Mycobacterium smegmatis* is porphyrin. *FEMS Microbiol. Lett.* **363** (2016).
37. W. Lee, B. C. VanderVen, R. J. Fahey, D. G. Russell, Intracellular *Mycobacterium tuberculosis* exploits host-derived fatty acids to limit metabolic stress. *J. Biol. Chem.* **288**, 6788-6800 (2013).
38. A. Martin, J. Daniel, The ABC transporter Rv1272c of *Mycobacterium tuberculosis* enhances the import of long-chain fatty acids in *Escherichia coli*. *Biochem. Biophys. Res. Commun.* **496**, 667-672 (2018).
39. T. Parish & N. G. Stoker, Use of a flexible cassette method to generate a double unmarked *Mycobacterium tuberculosis tlyA plcABC* mutant by gene replacement. *Microbiology* **146**, 1969-1975 (2000).

40. J. G. Nørby, Coupled assay of Na+,K+-ATPase activity. *Methods Enzymol.* **156**, 116–119 (1988).
41. K. Kiianitsa, J. A. Solinger, W.-D. Heyer, NADH-coupled microplate photometric assay for kinetic studies of ATP-hydrolyzing enzymes with low and high specific activities. *Anal. Biochem.* **321**, 266-271 (2003).

Acknowledgement

We thank Jia Fu Erh and Wei Shen Ho (National University of Singapore) for constructing plasmids and early affinity purification attempts. We are grateful to Beijing Genomics Institute (BGI) Research for providing DNA synthesis and assembly support. We thank Ross Tomaino (Taplin MS facility, Harvard Medical School) for help with protein identification.

Funding: Singapore Ministry of Education Academic Research Fund Tier 2 grants MOE2019-T2-1-128 and MOE000116 (SSC)

Author contributions:

Conceptualization: YC, SSC

Methodology: YC, SSC

Investigation: YC, YW, SSC

Visualization: YC, SSC

Supervision: SSC

Writing—original draft: YC

Writing—review & editing: YC, SSC

Competing interests: Authors declare that they have no competing interests.

Data and materials availability: All data are available in the main text or the supplementary materials.

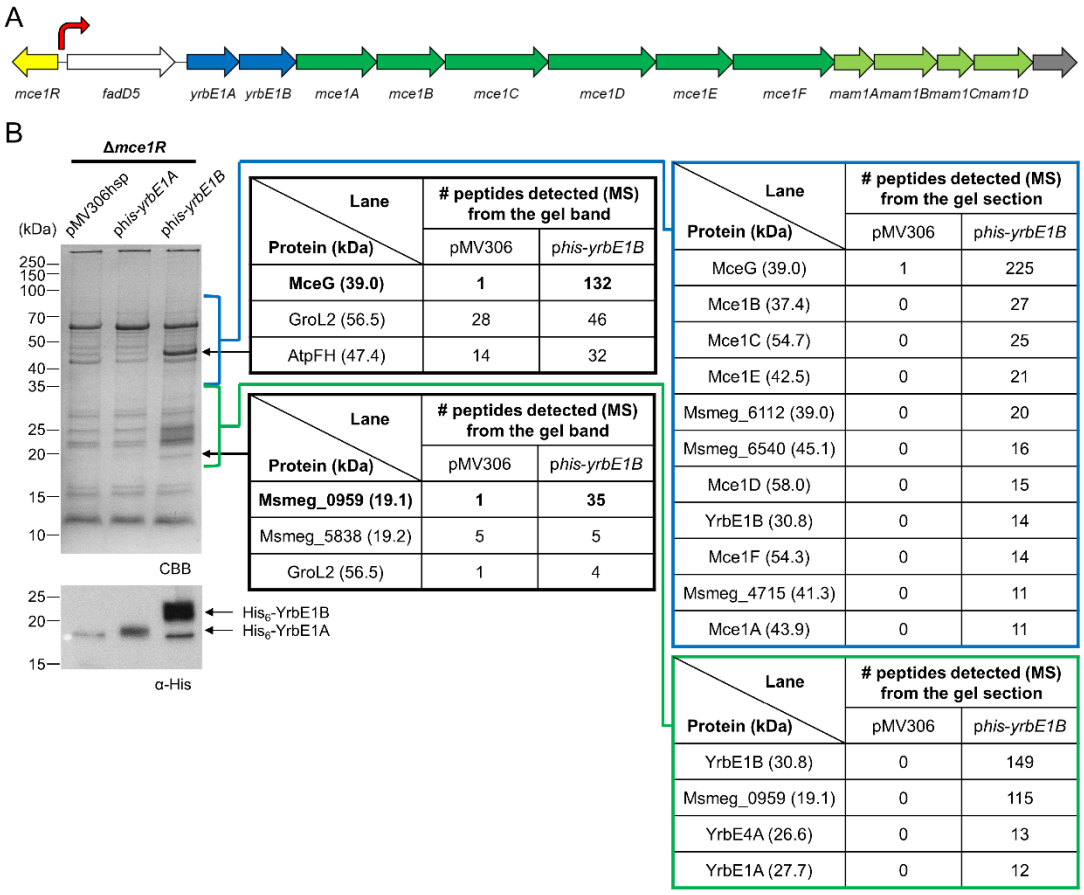

Protein (kDa) \ Lane	# peptides detected (MS) from the gel band	
	pMV306	*phis-yrbE1B*
MceG (39.0)	**1**	**132**
GroL2 (56.5)	28	46
AtpFH (47.4)	14	32

Protein (kDa) \ Lane	# peptides detected (MS) from the gel band	
	pMV306	*phis-yrbE1B*
Msmeg_0959 (19.1)	**1**	**35**
Msmeg_5838 (19.2)	5	5
GroL2 (56.5)	1	4

Protein (kDa) \ Lane	# peptides detected (MS) from the gel section	
	pMV306	*phis-yrbE1B*
MceG (39.0)	1	225
Mce1B (37.4)	0	27
Mce1C (54.7)	0	25
Mce1E (42.5)	0	21
Msmeg_6112 (39.0)	0	20
Msmeg_6540 (45.1)	0	16
Mce1D (58.0)	0	15
YrbE1B (30.8)	0	14
Mce1F (54.3)	0	14
Msmeg_4715 (41.3)	0	11
Mce1A (43.9)	0	11

Protein (kDa) \ Lane	# peptides detected (MS) from the gel section	
	pMV306	*phis-yrbE1B*
YrbE1B (30.8)	0	149
Msmeg_0959 (19.1)	0	115
YrbE4A (26.6)	0	13
YrbE1A (27.7)	0	12

Figure 1. Affinity purification with His$_6$-YrbE1B defines the composition of Mce1 complexes. (A) A schematic representation of the *mce1* genetic loci in *M. smegmatis*. Each straight arrow represents an individual gene. Lengths of the arrows are scaled to the lengths of the genes. The putative transcriptional regulator of the *mce1* operon is colored in *yellow*. *yrbE* genes are colored in *blue*, *mce* genes *dark green*, *mam* genes *light green*, and unrelated genes *grey*. The promoter position of the *mce1* operon is annotated with a turning arrow in *red*. **(B)** SDS-PAGE and α-His immunoblot analyses of proteins affinity-purified from *M. smegmatis* Δ*mce1R* cells expressing His-tagged YrbE1A (p*his-yrbE1A*) or YrbE1B (p*his-yrbE1B)*. pMV306hsp was used as the empty vector control. For protein identification from gel bands, the top three proteins detected in the p*his-yrbE1B* lane are listed. For protein identification from gel sections (blue: 35–90 kDa, green: 18–35 kDa), proteins with more than ten total peptides detected and significantly enriched in the p*his-yrbE1B* lane are listed. CBB, Coomassie brilliant blue.

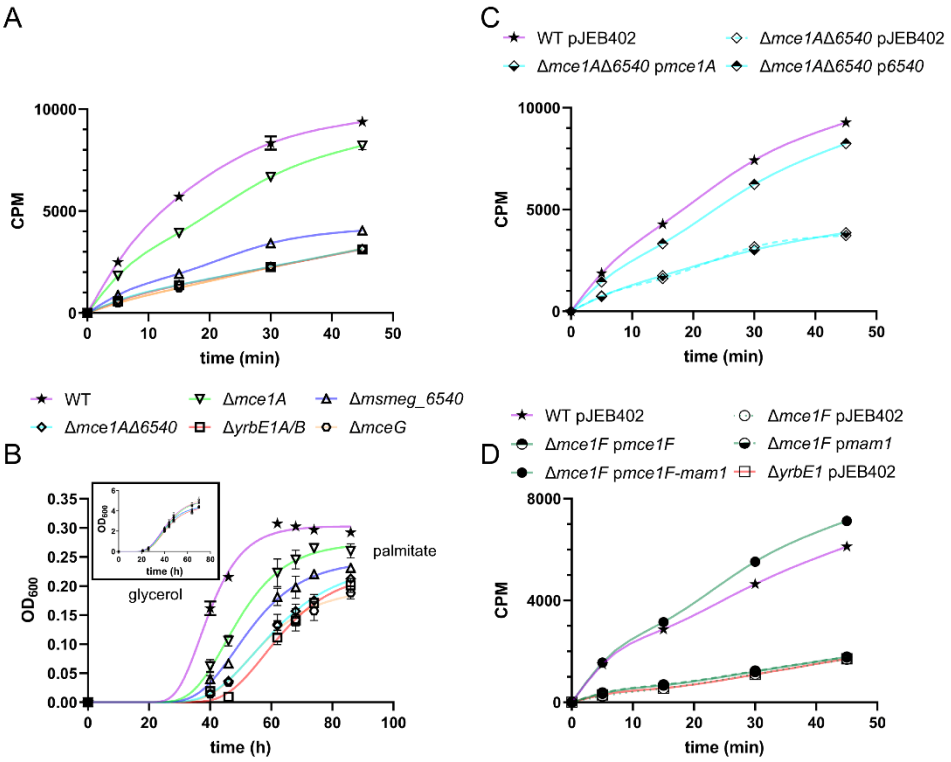

Figure 2. Msmeg_6540 and Mce1A are redundant components of the Mce1 system. (A) (C) (D) [^{14}C]-palmitic acid uptake kinetics of indicated *M. smegmatis* strains. Each data point (mean ± standard deviation) represents results from three technical replicates. The uptake profiles are representative of at least three independent experiments. **(B)** Growth curves of the same strains in **(A)** in Sauton's medium containing palmitate as the sole carbon source or (inset) 7H9 medium containing glycerol. Each data point (mean ± standard deviation) represents results from three biological replicates. In **(D)**, deletion of *mce1F* causes polar effects on downstream *mam1A–D* (*mam1*) genes, and can only be complemented by expressing *mce1F* together with *mam1* but not *mce1F* or *mam1* alone.

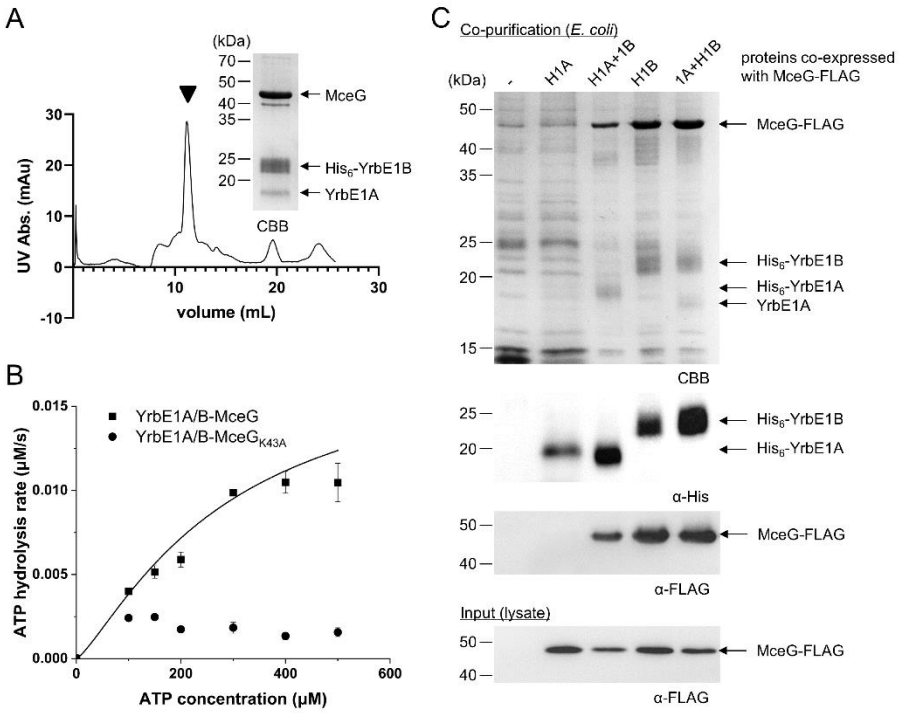

Figure 3. YrbE1A/B-MceG form a stable asymmetric complex with ATPase activity. (A) Size exclusion chromatographic profile of the purified complex comprising YrbE1A, His_6-YrbE1B and MceG. SDS-PAGE analysis of the peak corresponding to the complex (black arrowhead) is shown. **(B)** Enzyme-coupled ATPase assay of 0.1 μM YrbE1A/B-MceG and YrbE1A/B-$MceG_{K43A}$ in detergent micelles at 37 ºC. Average ATP hydrolysis rates from three technical triplicates were plotted against ATP concentrations, and fitted to an expanded Michaelis-Menten equation that includes a term for Hill coefficient (n). YrbE1A/B-MceG: $K_m = 284 \pm 311$μM, $k_{cat} = 0.184 \pm 0.125$ μM ATP s^{-1}/μM complex, n = 1.28 ± 0.57. The data for the mutant failed to fit to the equation with significant confidence. Each data point is shown as mean ± standard deviation. **(C)** SDS-PAGE and α-His/FLAG immunoblot analyses of proteins affinity-purified from *E. coli* cells over-expressing FLAG-tagged MceG together with either His_6-YrbE1A (H1A) with/without YrbE1B (1B) or His_6-YrbE1B (H1B) with/without YrbE1A (1A). CBB, Coomassie brilliant blue.

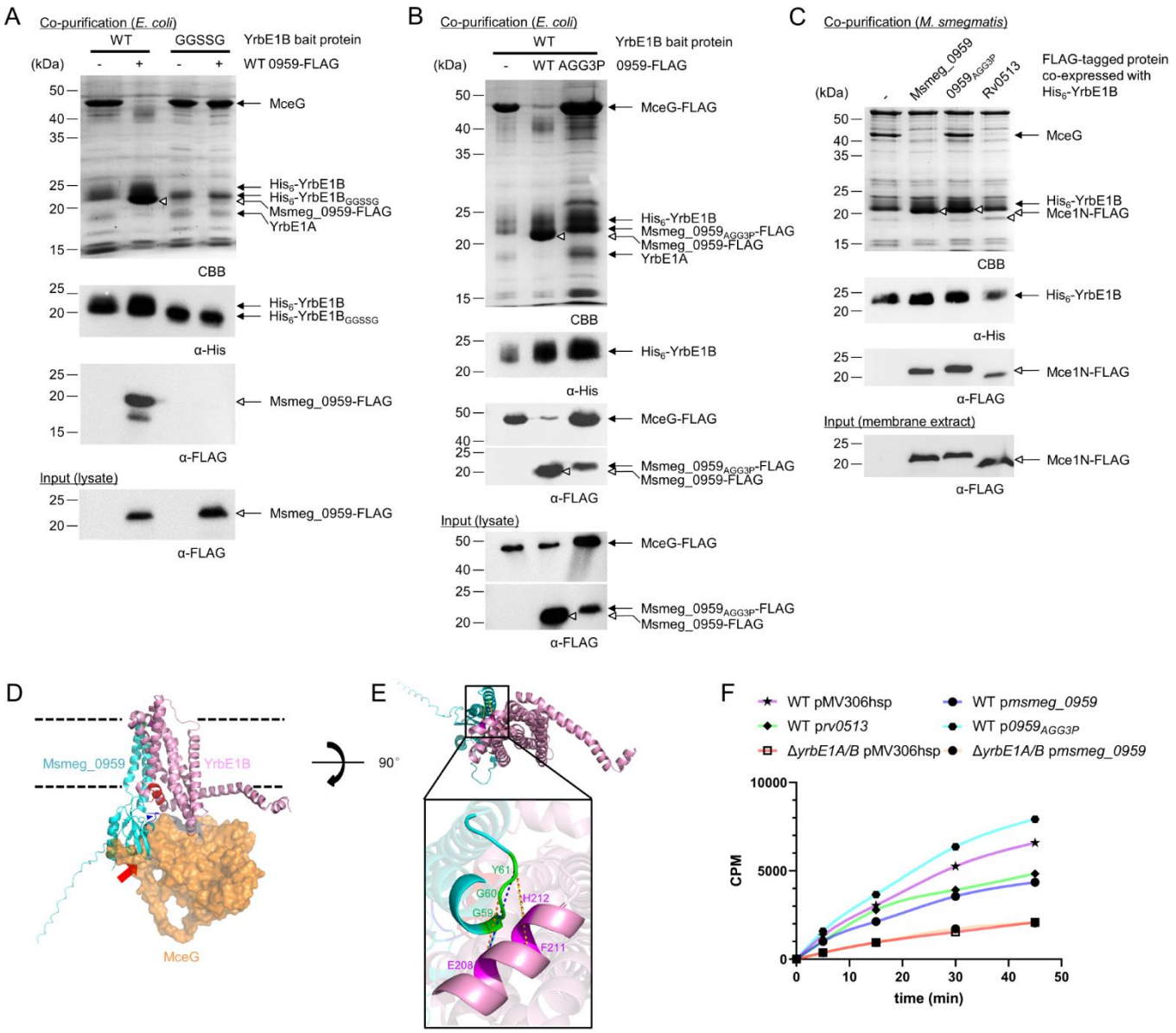

Figure 4. Msmeg_0959 negatively regulates the Mce1 transporter. (A) SDS-PAGE and α-His/FLAG immunoblot analyses of proteins affinity-purified from *E. coli* cells over-expressing YrbE1A, MceG, and either wild-type His_6-YrbE1B (WT) or the helix-to-loop mutant His_6-YrbE1B (GGSSG), in the presence (+) or absence (-) of Msmeg_0959-FLAG. **(B)** SDS-PAGE and α-His/FLAG immunoblot analyses of proteins affinity-purified from *E. coli* cells over-expressing YrbE1A, FLAG-tagged MceG, His-tagged YrbE1B together with FLAG-tagged wild type Msmeg_0959 (WT) or the loop-rigidified mutant (AGG3P). **(C)** SDS-PAGE and α-His/FLAG immunoblot analyses of proteins affinity-purified from *M. smegmatis* cells over-expressing His_6-YrbE1B as the bait protein together with Msmeg_0959, the loop-rigidified mutant (0959_{AGG3P}) or Rv0513 (Mce1N from *M. tuberculosis*). **(D)** An overlay of AlphaFold2 models of

YrbE1B (*pink*)-MceG (*orange* surface) and YrbE1B-Msmeg_0959 (*cyan*). The helix-to-loop mutation of YrbE1B located on the putative short helix at the YrbE1B-Msmeg_0959 interface is highlighted in *red*. The rigidified loop on the Msmeg_0959$_{AGG3P}$ mutant is highlighted in *blue* (with an arrowhead). The steric clash between MceG and Msmeg_0959 is indicated by a *red* arrow. Dashed lines represent arbitrary membrane boundaries based on hydrophobicity of the transmembrane regions. **(E)** A zoomed-in view of contact sites between YrbE1B and Msmeg_0959 revealed by disulfide crosslinks and mapped onto the AlphaFold2 model. Positions on YrbE1B and Msmeg_0959 that allowed disulfide formation between the two proteins are highlighted in *magenta* and *green*, respectively. **(F)** [^{14}C]-palmitic acid uptake kinetics of indicated *M. smegmatis* strains overexpressing different Mce1Ns. Each data point (mean ± SD) represents results from three technical replicates. The uptake profiles are representative of three independent experiments.

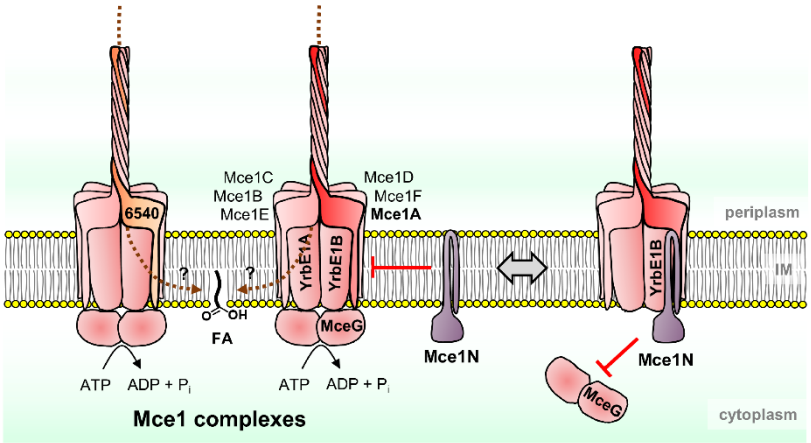

Figure 5. A proposed model of Mce1 complexes and their regulation by Mce1N. Mce1 complexes are ABC transporters for fatty acids, with YrbE1A/B as TMDs, MceG as NBDs, and heterohexameric MCE-domain proteins as SBPs. There are two variants of Mce1 complexes in *M. smegmatis*, each containing Msmeg_6540 or Mce1A in addition to Mce1B–F. The relative order of protomers within heterohexameric SBP complexes is indicated based on the AlphaFold2 models (Fig. S7B). Mce1N is a negative regulator of the Mce1 system; it specifically binds to YrbE1B and prevents its interaction with MceG.